Crystallization-induced suppression of intumescence in aqueous alkali silicates

Hamza Mohsin, Ekaterina Burov, Sandrine Tusseau-Nenez, Sébastien Maron, Lucie Devys, Thierry Gacoin, Emmanuelle Gouillart

Crystallization-induced suppression of intumescence in aqueous alkali silicates

Hamza Mohsin,[a, b] Ekaterina Burov,[a] Sandrine Tusseau-Nenez,[b] Sébastien Maron,[b] Lucie Devys,[c] Thierry Gacoin,[b] Emmanuelle Gouillart[c,*]

[a]Laboratoire Surface du Verre et Interfaces (SVI), UMR 125 CNRS/Saint-Gobain Research Paris, 93303 Aubervilliers, France

[b]Laboratoire de Physique de la Matière Condensée (PMC), CNRS, Ecole polytechnique, Institut Polytechnique de Paris, 91120 Palaiseau, France

[c]Saint-Gobain Research Paris, 93303 Aubervilliers, France

Email

hamzamohsin118@gmail.com

ekaterina.burov@saint-gobain.com

sandrine.tusseau-nenez@polytechnique.edu

sebastien.maron@polytechnique.edu

lucie.devys@saint-gobain.com

thierry.gacoin@polytechnique.edu

***Corresponding author:** emmanuelle.gouillart@saint-gobain.com (ph: +33 1 48 39 58 00)

Abstract:

Thermal properties of aqueous alkali silicates have been investigated to establish a fundamental understanding of the structural state of silicate network and its impact on intumescence, up to 450°C. Foaming behavior is dependent upon the type of alkali ion (Na, K, Li) as well as composition as evidenced from a combination of tools involving TGA, NMR

and XRD. Na silicates show extensive foaming, Li-silicates don't foam while K-silicates exhibit an intermediate behavior depending upon the starting state and heating kinetics. Crystallization is observed for K and Li-silicates but not in the case of Na-silicates. Crystallization appears to be a limiting factor for macroscopic structural expansion. Quantitative analysis of different species reveals the network to be relatively mobile in pre-dried Na-silicates, while a reduction in this mobility is seen for K-silicates due to a reduction of K ions and silanols in the amorphous phase at above 150°C, thus reducing the extent of foaming. In contrast, phase separation coupled with crystallization resulting in a complete exit of Li ions from the amorphous phase tends to suppress completely the intumescent nature.

Keywords: Silicates, Heat treatments, Intumescence/Foaming, Crystallization, Phase separation

1. Introduction

Intumescent property of alkali silicates has garnered extensive research and industrial attraction over the last decades particularly due to their thermal insulation properties at high temeprature – a source of fire-protection[1,2] in several construction materials including fire-resistant glasses. Furthermore, the ability of such silicate materials to act as strong binders (especially in geopolymers[3–5] and coatings[6–8]) makes them a potential candidate for a low-cost, stable and green alternative to several organic systems. Their foaming behavior in fire-protective systems has been the center of research especially when these silicates are applied as coatings. However, limitations on the availability of a solid in-depth understanding on the way these silicates behave thermally has led to their sluggish improvement that has hindered, over the years, their true potential for industrial systems.

Thus, a fundamental understanding of thermal evolution of aqueous alkali silicates has to be established for further exploitation of their properties.

Aqueous alkali silicates are commercially available soluble systems composed chemically of a silicate network dissolved in water. They are defined in terms of silica and alkali concentration denoted by the molar ratio M_2O/SiO_2 (where 'M' indicates the type of alkali ion i.e. Na, K or Li) and solid content. Thermal behavior of Na-based silicates has been quite extensively studied, focusing mainly on the macroscopic thermal evolution and microscopic properties at relatively lower temperatures. These systems have been found to exhibit considerable intumescence, associated to the removal of water.[9–13] However, only recently have we reported an in-depth understanding of the thermal evolution of Na-silicates by linking the macroscopic structural expansion to the changes induced at the microscopic scale.[11] Foaming/Intumescence is indeed a consequence of the release of proton-related species (present in the system as free water, solvating water molecules and silanols)[10,11] and is imparted due to the fact that the network remains relatively mobile on increasing temperature. A single activation energy (E_a) for water release is observed due to an equilibrium evolution of silanols and solvating water molecules. Furthermore, these systems also exhibit a xerogel-to-glass transition around 400°C.

Intumescence has also been reported as a property intrinsic to K-silicates – a consequence of dehydration[9,10,14,15]. However, there exists a lack of fundamental understanding on the exact thermal structural evolution in terms of water release and related phenomenon, and whether the intumescent behavior of K-silicates is fundamentally similar or different in comparison to other soluble alkali silicates. The starting solutions exhibit a structure, in terms of Q^n units obtained from ^{29}Si Nuclear Magnetic Resonance (NMR) spectroscopy, very

similar to that observed for Na-silicates with an increased amount of K ions leading to a depolymerization of the silicate network,[16] also reported for glasses[17–19] at room temperature. Heating such solutions to temperatures as high as 400°C is expected to change the network organization due to the release of the proton-related species resulting in microscopic network changes that in turn may influence the macroscopic behavior of the systems in terms of the extent of foaming. Extensive intumescence in K-silicate systems, comparable or even higher than Na-silicates[14], has been declared a consequence of the release of solvated water molecules[10] with an increased extent of expansion observed on increasing relative humidity. The foaming kinetics of a K-silicate gel[15] was suggested recently to be indeed a consequence of the release of free water followed by the evaporation of adsorbed water molecules and water from silanol groups in the range 150-350°C leading to subsequent removal of silanols until 550°C, which represented the maximum extent of intumescence. These reports estimate and link globally the release of water molecules, while lacking in terms of a reliable quantitative analysis using a combination of characterization tools. Furthermore, the ability of some K-silicate compositions to crystallize on thermal treatment[10,20] (leading to the formation of $KHSi_2O_5$) has also not been studied in the context of its influence on the extent of foaming.

Li-silicates (especially glass-based compositions), on the other hand, have been widely reported to exhibit crystallization on thermal treatment[21–27] with the formation of Li_2SiO_3 and $Li_2Si_2O_5$ as the most frequently observed phases depending upon the starting composition. Crystallization has also been observed for Li-silicate powders synthesized from gels; at room temperature[28] and on thermal treatments above 500°C[29,30] without any indication of intumescence or extensive macroscopic structural changes. In addition to crystallization, phase separation[23,27,31,32] is a characteristic property of Li-silicates which

is representative of the stability regime of aqueous systems, whose thermal behavior has not been fundamentally explored rather some studies on the mixture of solutions involving Li-silicates have been communicated where the addition of Li into K-silicates tends to reduce the extent of intumescence.[9,14] Pure Li-silicate solution is suggested to have little to no intumescence[9,33] even on keeping the system under a humid atmosphere followed by thermal treatment to 500°C and is considered to be the result of Li ions forming strong cross-links between polysilicate particles with the formation of $Li_2Si_2O_5$ crystals in the process.[9] On comparing the different alkali silicates, the degree of intumescence has in general been linked to the size of the cation in the sequence $K^+ >= Na^+ > Li^+$. But the absence of a comprehensive fundamental understanding in terms of quantitative evolution of different species in the system (protons, alkali ions) has rendered the available information less reliable. For instance, it is not yet clear how crystallization or phase separation may play a role in defining the thermal properties of alkali silicates. Hence, this necessitates the need to further investigate such systems from a structural point of view to bridge the gap in creating the link between intumescence and microscopic variations depending upon the type of alkali silicate and the corresponding composition.

Here, we report on a quantitative investigation approach, utilizing a combination of tools, to establish concrete ideas on the thermal evolution of aqueous K and Li-silicates starting from solutions and pre-dried powders all the way up to 450°C. K and Li-silicates are compared to results obtained on Na-silicates in our previous work.[11] The systems have been monitored visually to follow volumetric macroscopic changes in terms of their intumescent behavior as well as Thermogravimetric Analysis (TGA) has been performed to estimate the global evolution of water. Microscopic structural changes have been evaluated quantitatively using NMR spectroscopy while X-ray diffraction (XRD) has been utilized for estimating the degree

of crystallinity (DOC). This combinatory approach has allowed to compare the thermal behavior of different alkali silicates by creating a direct relation between intumescence, the evolution of proton-related species and the corresponding influence of crystallization.

2. Materials and Methods

2.1. Raw materials and sample preparation

Commercially available as well as lab prepared alkali silicate solutions were used as the starting materials. They have been defined in terms of their **Molar Ratio** as **M_2O/SiO_2** (where M corresponds to the type of alkali ion i.e. Na, K or Li). Solutions with two different molar ratios were used in all the cases and the respective composition of each solution is given in **Table 1**. Na-silicate extra pure solution (Na_2O/SiO_2=0.29) was purchased from Sigma-Aldrich, Na-silicate crystal 0095 solution (Na_2O/SiO_2=0.5) from PQ Corporation, K-silicate K 35 T (K_2O/SiO_2=0.29) and K-silicate Geosil 14517 (K_2O/SiO_2=0.59) from Woellner while Lithium polysilicate solution (Li_2O/SiO_2=0.2), Ludox As-30 colloidal silica (30 wt% suspension in H_2O) and Lithium hydroxide monohydrate (>=98%) from Sigma-Aldrich. K-silicate (K_2O/SiO_2=0.5) solution was prepared by mixing known amount of Ludox AS-30 in K-silicate Geosil 14517 (K_2O/SiO_2=0.59) with constant stirring until the solution becomes transparent. Li-silicate solutions (Li_2O/SiO_2=0.29 and 0.4) were prepared by adding known quantity of Lithium hydroxide monohydrate powder into Lithium polysilicate solution (Li_2O/SiO_2=0.2) with constant stirring at 60°C until the solutions become transparent. Note that the molar ratio of 0.4 represents the upper limit of stability for Li-silicate solutions.

Table 1: Composition (in wt%) of the starting alkali silicate solutions.

Alkali Silicate	M_2O (wt%)	SiO_2 (wt%)	H_2O (wt%)	Molar Ratio (M_2O/SiO_2)
Na	8.25	27.75	64	0.29
	13.75	27.25	59	0.5
K	11	24	65	0.29
	17	23	60	0.5
Li	2.6	17.8	79.6	0.29
	3.4	17.3	79.3	0.4

Alkali silicate dried powders were prepared by heating the initial solutions in an oven at 150°C for 17 h to remove maximum amount of free water and limit the extent of intumescence while performing further analyses. For our investigations, further thermal treatments were achieved at 275°C, 350°C, 400°C and 450°C at a heating rate of 5°C/min for 2 h each. Obtained powders were ground and stored in sealed glass vials.

2.2. Characterization tools

2.2.1. Visual monitoring

The impact of thermal treatment on bare solutions was investigated visually by comparing the different silicates. 0.5 mL of each solution in an uncapped glass vial was heated in an oven to 350°C for 30 min. Pictures were acquired using a smartphone camera before and after thermal treatment. The extent of volumetric expansion in terms of intumescence was measured using a 12-inch measuring scale.

For a precise in-situ monitoring on thermal evolution of a powder pellet, a hot-stage microscope equipped with a 10X objective was utilized to record a video by capturing an image every second on ramping up to 400°C. Further details of the experimental parameters and the setup can be found in ref [11].

2.2.2. Thermal analysis

Thermogravimetric analysis (TGA) was performed using a NETZSCH STA 409 Thermal Analyzer for obtaining mass loss curves up to 1200°C to monitor the evolution of leftover water or silanols with temperature in Na-silicate powders pre-dried at 150°C. An alumina crucible was used as the container and a moisture-free atmosphere was provided by continuously flowing N_2/O_2 gases in nearly equal volume. The measurement was repeated twice. Only small quantities of samples could be analyzed for Na and K-silicates, typically 15 mg of the powder pre-dried at 150°C, because of expected intumescence that led to some inconsistencies in the RT-150°C temperature range. 50 mg powder was used for the analysis of Li-silicate pre-dried systems as these don't show any intumescence.

2.2.3. Nuclear Magnetic Resonance Spectroscopy

Liquid-state ^{29}Si NMR: The structure of Na-silicate solutions in terms of Q^n units was analyzed using liquid-state ^{29}Si NMR. Spectra were recorded at 59.63 MHz on a 300 MHz AVANCE II Bruker spectrometer with a BBO probe. A $\pi/2$ pulse was used with a repetition delay optimized at 5 s. 30 vol% heavy water (D_2O) was added to the samples for locking. All ^{29}Si chemical shifts were referenced to tetraethoxysilane (TEOS) as external reference [Chemical shift (Si)=-82 ppm vs TMS]. The contribution of glass tube was corrected by subtracting the spectrum of empty tube from the final spectrum of silicate solutions. The relative proportion of Q^n units was determined by integrating the area under the curve of each peak for an exact quantification of the various species.

Solid-state MAS ^{29}Si NMR: The samples treated at different temperatures were analyzed with solid-state magic angle spinning (MAS) NMR experiments. The 1D ^{29}Si NMR spectra were acquired at 71.53 MHz on a Tecmag Apollo360 spectrometer equipped with a 4 mm

Bruker probe head operating at a spinning frequency (ν_{rot}) of 15 kHz. The acquisitions were performed with a 3.55 µs pulse length (corresponding to a $\pi/2$ flip angle), 3000 transients and a repetition delay of 20 s. The repetition delay was optimized by going up to 2000 s but that does not provide higher signal intensity. ^{29}Si chemical shifts were referred to TEOS at -82 ppm. Deconvolution of the ^{29}Si NMR spectra was performed using the Dmfit software[34] with Gaussian fitting function because of the chemical shift distribution of amorphous structures.

2.2.4. X-Ray Diffraction

Powder X-ray diffraction (XRD) experiments were carried out on a high-resolution D8 Advance Bruker AXS (Germany) θ-θ powder diffractometer equipped with the LynxEye XE-T detector (1D mode, maximum detector opening), automatic anti-scatter screen position and a Cu radiation ($K\alpha_1$ = 1.5406 Å and $K\alpha_2$ = 1.5445 Å). Samples were analyzed at room temperature using 2.5° Soller slits and a divergence slit of 0.6° in the 5-70° 2θ range with a step size of 0.025° at 1 s/step. Phase identification was performed with the Bruker AXS DIFFRAC.EVA (V5) software using the PDF2 (release 2004) database. Deconvolution of the XRD diffractograms was carried out on Bruker AXS TOPAS (V6) software. The fundamental parameter approach was used to model the optical contribution and the emission profile of the X-Ray tube was established using LaB_6 NIST standard (Standard Reference Material 660a, cell parameter = 0.41569162 nm – 0.00000097 nm at 22.5 °C). The background was described using a Chebychev polynomial. Since the diffractograms were a combination of amorphous and crystalline character, split pseudo-voigt (SPV) function was used to define both the amorphous bump (using the single peak method) and crystalline peaks corresponding to the different phases detected. The Crystallographic Information File (.cif) for each phase was downloaded from the Crystallography Open Database (COD)[35],

Inorganic Crystal Structure Database ICSD and MaterialsProject.[36] For the Rietveld refinements, cell parameters, microstructure (double-Voigt approach, only crystallite size refined) and preferred orientation (March-Dollase model) were fitted whereas atomic positions and site occupancies were fixed according to the .cif files used.

3. Results and Discussion

3.1. Global thermal evolution

3.1.1. Visual monitoring

Aqueous alkali silicates contain a silicate network dissolved in water as represented schematically in **Figure 1**(a). These solutions are composed of several proton-related species namely free water, solvating water (molecules H-bonded to alkali ion or network protons) and silanols.[10,11] Thermally treating these silicate solutions results in the removal of water directly influencing the macro and microscopic structural properties (**Figure 1**(b) shows a schematic illustration of the expected state of the network on dehydration).

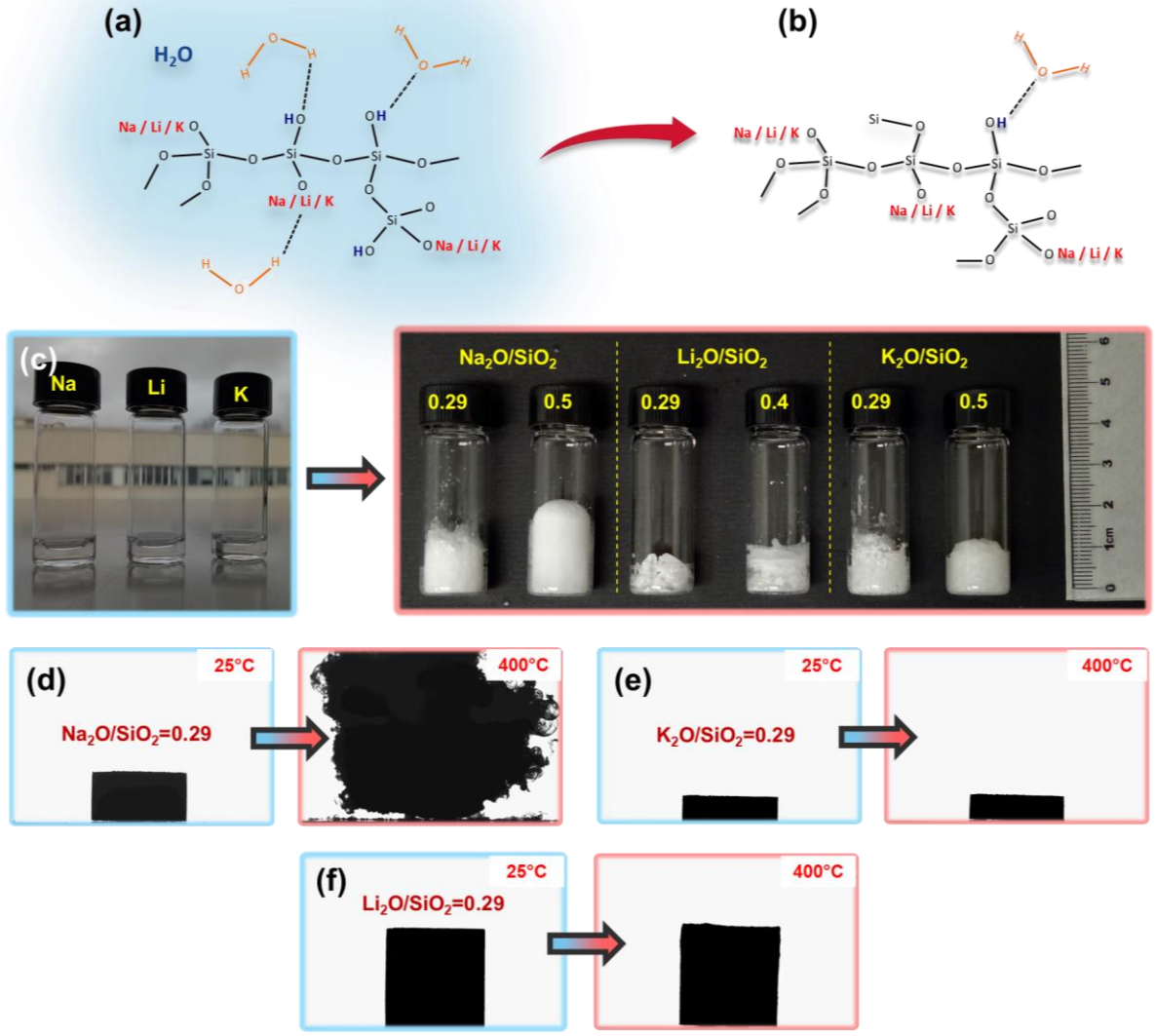

Figure 1: Effect of heating aqueous alkali silicates at 350°C for 30 min at 5°C/min (schematic illustration of microstructure (a) before and (b) after heating) showing (c) extensive intumescence in Na-silicates, no expansion in Li-silicates while intermediate intumescence in K-silicate solutions. The image series (d, e and f) shows thermal evolution of pre-dried powder pellets for Na at 10°C/min, K at 10°C/min and Li-silicate at 5°C/min, respectively, with a molar ratio 0.29 prepared by pre-drying the solutions at 150°C for 17 h.

Visual investigation shows that heating such solutions results in macroscopic structural changes intrinsic to the type and composition of alkali silicate. Na-silicate solutions, on direct heating to 350°C, show extensive structural expansion referred to as 'foaming' or

'intumescence' as shown in **Figure 1**(c). Li-silicates don't foam at all leaving behind a non-intumesced dried powder while K-silicates show an intermediate structural expansion i.e. in-between Na and Li-silicates. Furthermore, the composition of these silicate solutions in terms of the molar ratio also impacts the foaming/drying behavior. The extent of volumetric expansion up to 350°C for each composition at a heating rate of 5°C/min is listed in **Table 2**. A 400% expansion is observed for solution with higher Na concentration (Na_2O/SiO_2=0.5) as compared to 225% observed in Na_2O/SiO_2=0.29, despite a lower initial water content for the molar ratio of 0.5 (see **Table 1**). K-silicates show a roughly similar expansion with 175% for solution with a molar ratio of 0.29 and 200% for 0.5, respectively. This foaming behavior of aqueous silicates is linked to the release of water content from the system leading to a more condensed network at the microscopic scale. Note that the extent of foaming is reproducible in all the cases except K_2O/SiO_2=0.29 solution which, sometimes, may exhibit splashing making it difficult to record the exact values.

Table 2: Extent of macroscopic expansion (%) at 5°C/min for different aqueous alkali silicates.

Alkali Silicate	Molar Ratio (M_2O/SiO_2)	Expansion at 350°C (%)
Na	0.29	225
	0.5	400
K	0.29	175
	0.5	200
Li	0.29	0
	0.4	0

The image series **Figure 1**(d, e and f) shows the evolution of pre-dried powder pellets of the different alkali silicates, having a molar ratio 0.29, under a hot-stage microscope (corresponding videos are given in **SI**). The behavior of the solutions appears to be slightly

different than that of the powders (depending upon the type of alkali silicate) obtained by pre-dying the solutions at 150°C for 17 h. These powders would be referred to as 'pre-dried' throughout the reported work. It has to be noted here that pre-drying is a necessary step in our systems due the limitations posed by various characterization tools used for acquiring the relevant structural information. Na_2O/SiO_2=0.29 powder pellet shows an extensive foaming on heating to 400°C as shown in **Figure 1**(d), while no volumetric expansion is observed for the pre-dried K_2O/SiO_2=0.29 powder pellet (see **Figure 1**(d)) suggesting that either all the foaming has occurred during the pre-drying step or the structure of the system is changing (e.g. crystallization as shown in Figure S1) with time such that it tends to prevent foaming at elevated temperatures. Li_2O/SiO_2=0.29 pellet doesn't show any extensive evolution either, as shown in **Figure 1**(e), consistent with the evolution of the solutions.

Keeping in view the experimental limitations associated with characterization of solutions, the discussion from this point onwards focuses on the evolution of pre-dried powders. These are expected to have undergone enough structural changes during the drying step to influence their macroscopic behavior as discussed above. Thus, it is necessary to conduct a thorough investigation of the structural evolution upon thermal treatment in order to clarify the differences in the evolution of the different alkali silicates in terms of the removal of water as well as any other phenomenon intrinsic to the type of system studied.

3.1.2. Water content variation

For a global picture of the water content evolution on thermal treatment, TGA measurements were performed on pre-dried alkali silicate powders. The mass loss curves for all the compositions acquired at a heating ramp of 10°C/min are shown in **Figure 2**(a, b). Both the Na-silicate compositions as well as K_2O/SiO_2=0.5 show a rapid and homogeneous

release of water content. In contrast, K_2O/SiO_2=0.29 and Li-silicate pre-dried powders tend to evolve in a slightly different manner in the sense that dehydration seems to occur in steps over the temperature interval studied (see **Figure 2**(b)).

One commonality among all the systems is that on increasing the alkali concentration, a different onset temperature of mass loss is observed i.e. higher alkali content silicates tend to start losing water at lower temperatures e.g. Na_2O/SiO_2=0.29 has a rapid dehydration temperature of 210°C while 175°C is observed for Na_2O/SiO_2=0.5. Similarly, K_2O/SiO_2=0.29 sees a considerable drop in the TGA curve around 220°C and the system seems to retain water till higher temperatures while the temperature for the start of dehydration drops to around 190°C for K_2O/SiO_2=0.5 followed by a gradual evolution as observed in Na-silicates. Li-silicates also show a similar behavior in terms of the onset in temperature for the start of dehydration with a higher value i.e. 200°C seen for Li_2O/SiO_2=0.29 (the mass loss behavior seems to be slightly different when compared to Na or K silicates). This difference in onset of dehydration temperature is linked to the fact that the network tends to be more mobile on increasing the alkali concentration as well as retaining a higher water content[11,37] resulting in a reduced onset temperature of dehydration as observed especially in the case of Na and K-silicates (see Figure S2). This behavior is similar to glass systems where a reduction in the glass transition (T_g) of silicate melts is observed when the amount of available silanols in the systems increases rendering the network more mobile.[38]

To further investigate the thermal evolution of these silicates, activation energy (E_a) values were calculated from the TGA mass loss curves by plotting the water content versus inverse of temperature as shown in **Figure 2**(c, d) for K and Li-silicates. These values have been

calculated considering that removal of silanols (given by eq. 1) may be the dominant reaction for the release of proton-related species in the network.

$$2SiOH \rightleftharpoons Si - O - Si + H_2O_{atm} \quad (1)$$

The reaction constant (k) can thus be expressed as:

$$k = \frac{p[H_2O]}{c[SiOH]^2} = A \exp\left(\frac{-E_a}{RT}\right) \quad (2)$$

where 'p' is the partial pressure, 'c' the concentration, 'A' the pre-exponential factor, 'E_a' the activation energy, 'R' the gas constant (8.3145 J.mol^{-1}.K^{-1}) and 'T' the temperature in K. Considering that the partial pressure of water is fixed by a large atmospheric reservoir, therefore, making it constant, the E_a is linked to protons as:

$$[SiOH] \sim \exp\left(\frac{E_a}{2RT}\right) \quad (3)$$

Na-silicates have shown an Arrhenius evolution (below 500°C) with E_a values approaching 30 kJ.mol^{-1} for both the molar ratios[11] (as shown in Figure S3) which has been previously observed for glass melts.[39,40] The existence of a single E_a is a consequence of an equilibrium where silanols are released first followed by their conversion into solvating water molecules which then leave the system due to evaporation.[11] K and Li-silicates, on the other hand, tend to show multiple activation energies. Therefore, the evolution of mass loss corroborates the visual inspection of macroscopic foaming, with a different behavior for Na-silicates on the one hand, and K- and Li-silicates on the other hand.

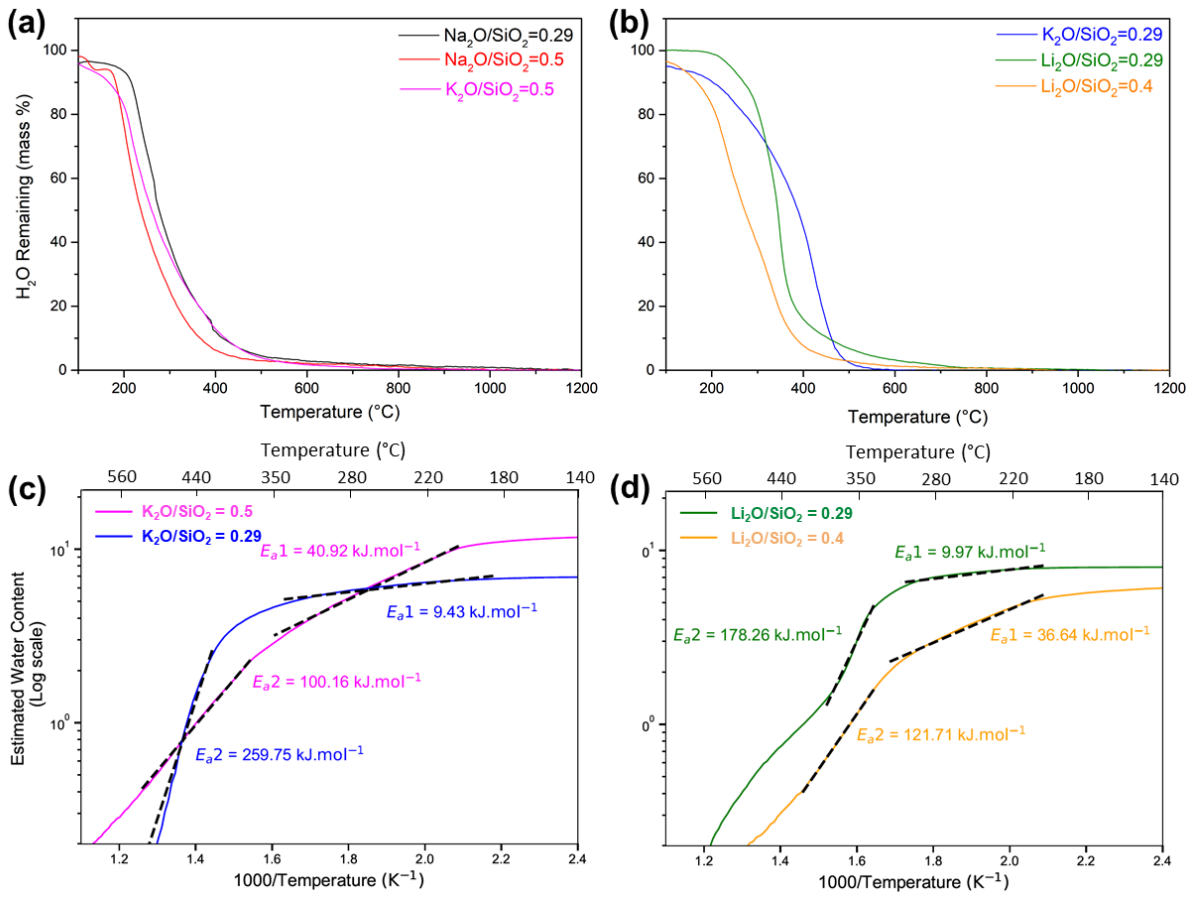

Figure 2: (a, b) TGA mass loss evolution (in terms of total water content) for two different molar ratios of alkali silicate powders pre-dried at 150°C (all the measurements were acquired at a heating ramp of 10°C/min), Activation energy (E_a) obtained from TGA mass loss data indicating (c) Arrhenian behavior for K_2O/SiO_2=0.5 while (c, d) multiple values for K_2O/SiO_2=0.29 and Li-silicate pre-dried powders.

K_2O/SiO_2=0.5 has an E_a of 40.92 kJ.mol^{-1} up to 350°C suggesting a behavior very similar to that observed for Na-silicates. However, the value increases to 100.16 kJ.mol^{-1} above 370°C. Similar behavior but different E_a values are observed for K_2O/SiO_2=0.29 as shown in **Figure 2**(c) with a very small value of 9.43 kJ.mol^{-1} for water release seen up to 340°C followed by 259.75 kJ.mol^{-1} above 400°C. Li-silicates, again, show multiple values of E_a (two or even more), however, the temperature range is slightly shifted to lower temperatures. **Figure 2**(d) shows the E_a (in the range 200-300°C) to be 9.97 and 36.64 kJ.mol^{-1} for Li_2O/SiO_2=0.29 and Li_2O/SiO_2=0.4, respectively, while values above 100 kJ.mol^{-1} are observed in the range 340-

390°C. The existence of these multiple E_a values happens to be a consequence of microscopic structural changes linked to the release of water and an underlying phenomenon related to crystallization or phase separation not at all observed in Na-silicates below 500°C, where the network happens to be mobile enough to let the water molecules escape resulting in extensive foaming.

Binary phase diagrams (in terms of total water and total amorphous composition) for Na and K-silicates calculated from FactSage[41] (see **Figure 3**) show the temperature range for the existence of different phases upon dehydration. Calculations could not be made for Li-silicates due to unavailability of relevant information in the FactSage database. Phases referred to as 'Hydrated Amorphous' are indicative of the amorphous alkali silicate network that is independent of free water but is composed of network silanols and solvating water molecules. 'Vapor' corresponds to the water molecules that are released on thermal treatment while 'Liquid' is representative of free water in the system. Starting solution compositions are shown by the blue dots while specific TGA data points, corresponding to temperatures studied for quantitative analysis later on, are marked with black points. Note that the black points at 150°C in **Figure 3** are the starting points for TGA measurements and represent the water content in the pre-dried silicate powders.

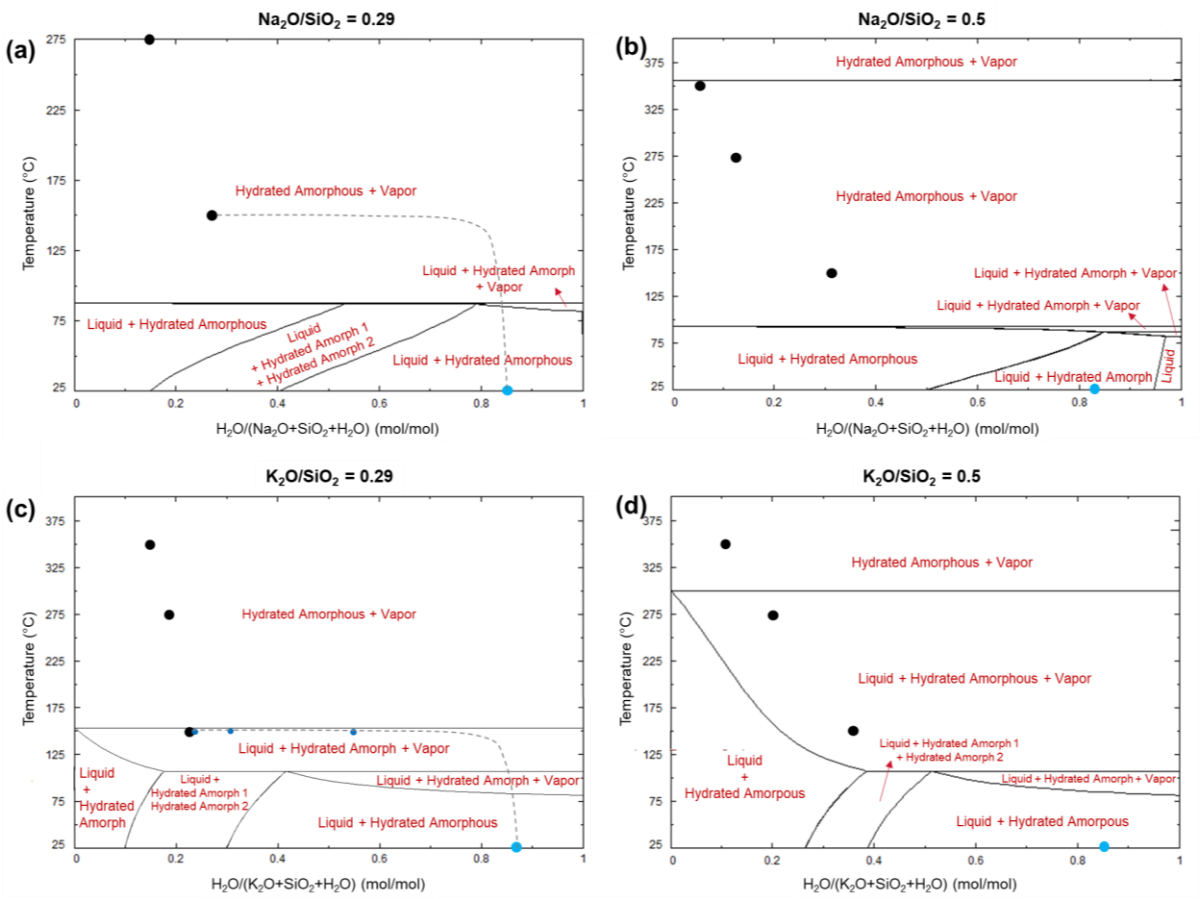

Figure 3: Binary phase diagram for (a) Na_2O/SiO_2=0.29, (b) Na_2O/SiO_2=0.5, (c) K_2O/SiO_2=0.29 and (d) K_2O/SiO_2=0.5, obtained from FactSage[41] at 1 atm, indicating the presence of various phases as a function of temperature and mole fraction of H_2O. Light blue points on the diagrams are representative of the starting solutions while black points indicate the TGA evolution of pre-dried powders prepared at 150°C (by drying solutions for 17h), whereas dashed grey line in (a) and (c) is just a rough assumption indicating the loss of water on drying the starting solutions with dark blue points showing the leftover water content after 15 min, 1 h 40 min and 3 h drying at 150°C. Note also that these diagrams were calculated without considering the possibility of crystallization.

Starting alkali silicate solutions are in the hydrated amorphous regime as shown by the ternary phase diagrams in Figure S4 suggesting the system to be composed of an amorphous alkali silicate network dissolved in water. Dehydration of the proton-related species and the extent of foaming observed is expected to be dependent upon the stability of different phases in the relevant temperature range. Extensive foaming observed in Na-silicates above

150°C stems from the fact that the system is in the range where the network is in equilibrium with evaporating water as shown by the black points at and above 150°C in **Figure 3**(a, b). This means that water can escape rather easily at temperatures as low as around 90°C which is quite close to the boiling point of water. The dehydration in K_2O/SiO_2=0.29 is somewhat similar to Na-silicates above 150°C but the pre-drying at 150°C, on viewing from the phase diagram in **Figure 3**(c), implies the system to be in a state where the thermodynamic stability of water may be higher than that observed for Na-silicates suggesting it to be more hygroscopic in terms of rheological aspects and thus might influence the foaming behavior. K_2O/SiO_2=0.5 (very hygroscopic), in contrast, has a broad temperature range 100-300°C within which 'Liquid + Hydrated Amorphous + Vapor' co-exist as shown in **Figure 3**(d) indicating that the pre-dried powder at 150°C may not be a xerogel, or a dried gel, and the extent of foaming is reduced as compared to Na-silicates due to the relatively stable nature of proton-related species.

Differences in the foaming/thermal behavior of alkali silicates can further be linked to the network mobility, which depends on the rheology of the material, and therefore of the presence of a crystalline phase or several amorphous phases (as during phase separation).

Thus, in order to investigate extensively the role a varied water content evolution and crystallization or phase separation plays in reducing or completely suppressing intumescence, a thorough quantitative structural investigation is required for understanding how the structural mobility is limited on thermal evolution in the case of K and Li-silicates.

3.2. Quantitative analysis

3.2.1. Evolution of Q^n units

Thermal treatment of aqueous alkali silicates is responsible for the induction of microscopic structural changes linked to the removal of proton-related species. These structural changes in the network are in turn responsible for the kind of foaming/intumescent behavior observed visually. Aqueous alkali silicates can be structurally characterized based on the existence of various Q^n units that are the building blocks of the microscopic network. A Q^n unit corresponds to a Si-centered tetrahedron linked to n other such tetrahedra; oxygens linking together such tetrahedra are called *bridging* oxygens while other oxygens, linked to alkali or protons, are *non-bridging* oxygens (NBOs). Q^n species, identified by ^{29}Si liquid-state NMR, are given by the spectra of Na, K and Li-silicate solutions shown in **Figure 4**. Each spectrum shows the existence of multiple peaks which may correspond to Q^0, Q^1, Q^2, $Q^{2\Delta}$ (cyclic species of Q^2), Q^3, $Q^{3\Delta}$ (branched cyclic species of Q^3) and Q^4 depending upon the composition studied.[42–49] For each molar ratio, the structure of Na and K-silicate solutions is very similar (see **Figure 4**(a, b)). Initially, for a molar ratio of 0.29, Q^0, Q^1, Q^2, $Q^{2\Delta}$, Q^3 and Q^4 are the species observed. On increasing the concentration of Na or K in the solution i.e. to achieve a molar ratio of 0.5, the network tends to depolymerize resulting in the conversion of higher Q^n units into lower ones along with the formation of $Q^{3\Delta}$ species. Li_2O/SiO_2=0.29 has a structure in solution similar to Na and K-silicates, although it is slightly more depolymerized, with less Q^4 species. However, addition of further Li doesn't seem to impact much the structure as observed for Li_2O/SiO_2=0.4[49] and shown in **Figure 4**(c), suggesting either an already saturated network or the presence of LiOH that may or may not be H-bonded to the network.

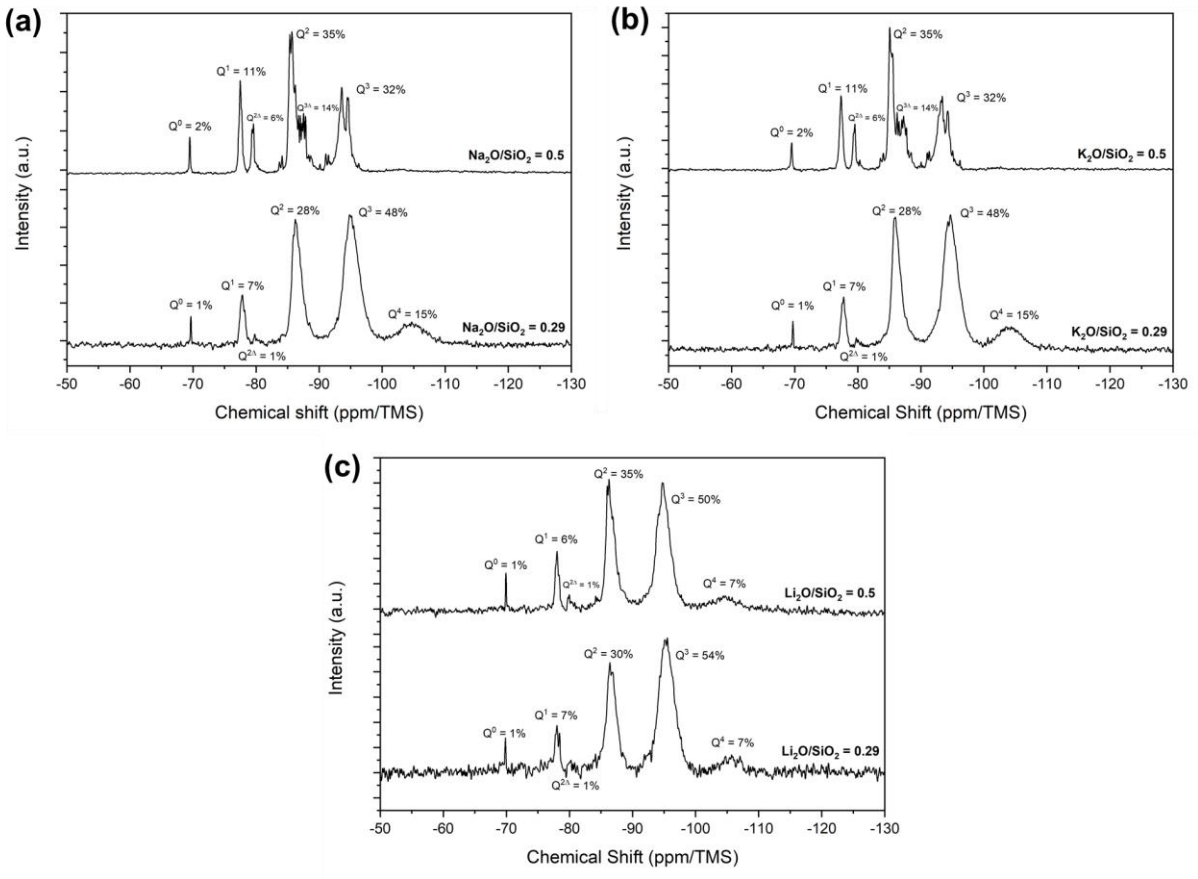

Figure 4: ^{29}Si liquid-state NMR of (a) Na, (b) K and (c) Li-silicate solutions indicating the existence of different Q^n units. Assignment has been done according to literature.[42–49]

On thermal treatment of these solutions, the network distribution is expected to change as a consequence of changing water content that is expected to give a concrete information on the link between the state of the network and macroscopic evolution in terms of foaming behavior. In order to explore quantitatively the thermal evolution of these silicates, solid-state ^{29}Si NMR was utilized to follow the evolution of Q^n units. **Figure 5** shows the behavior of K and Li-silicate with a molar ratio of 0.29. Broad bands can be seen due to the glassy nature of the samples, which have to be deconvoluted to extract quantitative information on the relative distribution of various Q^n units. Deconvolution of the broad band indicates broad peaks representative of the amorphous content as well as sharp peaks shown in orange (see **Figure 5**(a, b)) resulting from the fact that the samples have crystallized (details

on XRD data are discussed in section **3.2.2**). For both K and Li-silicates, the system globally tends to move towards a more polymerized state evident from the fact that the fraction of Q^4 in the system increases with temperature.

At 150°C, K_2O/SiO_2=0.29 is already crystallized evident from the appearance of two crystalline polymorphs of $KHSi_2O_5$, namely, monoclinic denoted by Q^3_{cM} with a fraction of 15% while orthorhombic by Q^3_{cO} contributing 45% to the total sum. On increasing the temperature, a variation in the contribution of these polymorphs is observed i.e. the orthorhombic crystalline phase increases while monoclinic reduces and melting of the crystalline phases is seen at 450°C where the crystalline peaks are no more visible (also confirmed from XRD discussed later). Globally, Q^3 tends to reduce while Q^4 increases suggesting network polymerization as a function of temperature. **Figure 5**(c) gives a comparison of the two molar ratios of K-silicate. Note that the data points for K_2O/SiO_2=0.5 have been extracted from Figure S6(a) which also indicates a tendency towards network polymerization on increasing temperature. Q^2 reduces while Q^3 increases suggesting a loss of proton-related species on thermal treatment as shown in **Figure 5**(c). This system seems to not crystallize using the same pre-drying steps used for other silicates. However, drying the solutions for longer durations i.e. 1 week at 150°C is necessary to be able to extract information from solid-state NMR as the powders dried for 17 h were very hygroscopic leading to experimental issues.

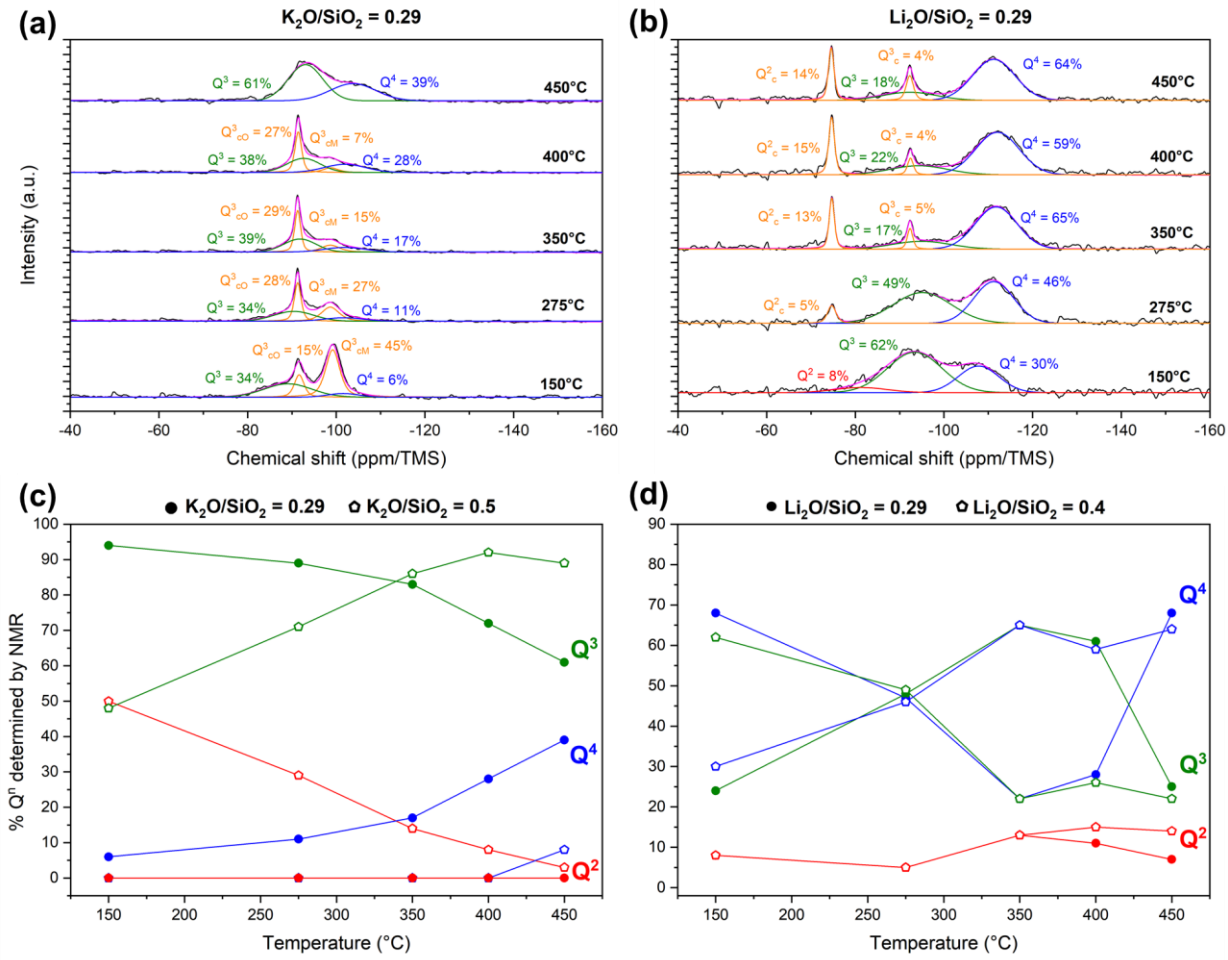

Figure 5: Evolution of Q^n units for (a) K_2O/SiO_2=0.29 and (b) Li_2O/SiO_2=0.29 powders dried at different temperatures determined from ^{29}Si solid-state NMR spectroscopy (note that the sharp deconvoluted peaks in orange represent crystalline phases i.e. Q^3_{cO} for orthorhombic $KHSi_2O_5$ and Q^3_{cM} for monoclinic KHSi2O5 in the case of K, while Q^2_c for orthorhombic Li_2SiO_3 and Q^3_c for orthorhombic $Li_2Si_2O_5$ phase in Li-silicate), comparison of Q^n units evolution for the two molar ratios of (c) K-silicates and (d) Li-silicates with '●' representing the molar ratio of 0.29 while 'o' for K_2O/SiO_2=0.5 and Li_2O/SiO_2=0.4, respectively. The data for the K_2O/SiO_2=0.5 has been extracted from Figure S6 and for Li_2O/SiO_2=0.4 from Figure S7.

Li-silicates show a completely amorphous behavior at 150°C with crystalline peaks appearing at 275°C and above – Q^2_c representing Li_2SiO_3 while Q^3_c indicating the presence of $Li_2Si_2O_5$ observed also in binary Li-silicate glasses with the same composition.[50] Crystallization of the system increases as a function of temperature for both the molar ratios suggesting the existence of the disproportionation reaction: $2Q^3$(glassy) ↔ Q^2 (crystalline) + Q^4 (glassy).

Globally, as observed in case of Na[11] and K-silicates, the system tends to evolve towards a more condensed state on increasing temperature. Dissolution of the crystalline phase is observed for Li_2O/SiO_2=0.4 at 450°C similar to what has been reported for glasses at very high temperatures (800°C) [50] suggesting a behavior relatively similar to binary glasses, though not a lot of information is available on such glass systems with added water content.

In essence, Na, K and Li-silicates all tend to polymerize as a consequence of condensation of proton-related species. However, the existence of crystallization in both K and Li-silicates influences the microstructure of the systems. The viscosity or rheological properties are expected to be directly influenced by crystallization, impacting the way these silicates behave macroscopically in terms of intumescence. ^{29}Si solid-state NMR has given us a more in-depth information on the degree of polymerization of the network. Further quantification is, however, required to probe the state of the silicate network in terms of both the evolution of proton-related species and the exact impact of crystallization on the network.

3.2.2. Crystallization behavior

To further investigate the crystallization behavior of K and Li-silicates for establishing a quantitative understanding, diffractograms were obtained from powder XRD shown in **Figure 6**. The patterns for K_2O/SiO_2=0.29 suggest the existence of a combination of amorphous and crystalline character as represented in **Figure 6**(a) and also evident from the ^{29}Si NMR discussed previously. Two different polymorphs exist as discussed in the section **3.2.1** i.e. monoclinic and orthorhombic $KHSi_2O_5$.[10] The XRD patterns have been deconvoluted (using Rietveld refinement approach) to extract quantitative information on the exact amount of crystalline and amorphous phases that has been further utilized to probe the quantity of alkali in the amorphous and crystalline phases, respectively.

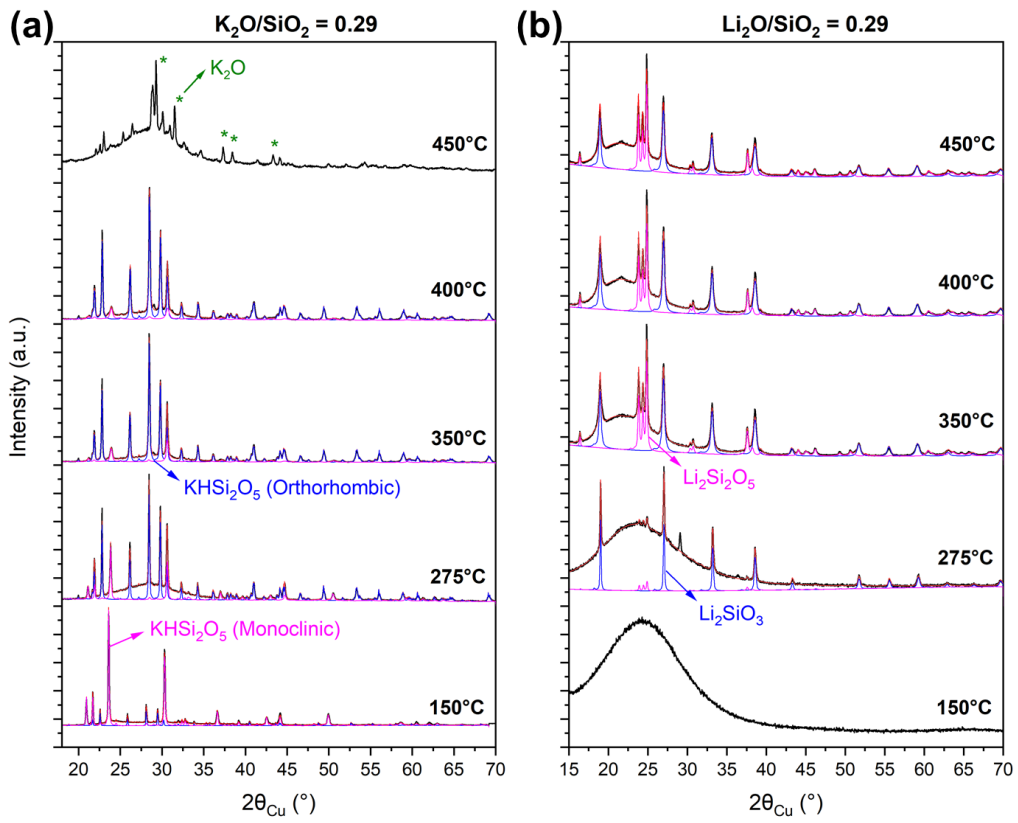

Figure 6: XRD data showing a combination of amorphous and crystalline phases in (a) K_2O/SiO_2=0.29 with two polymorphs of $KHSi_2O_5$ and (b) Li_2O/SiO_2=0.29 indicating the presence of crystalline orthorhombic Li_2SiO_3 and $Li_2Si_2O_5$. Deconvolution of the peaks allows for quantification of the different phases/species through Rietveld refinement method. Detailed parameters of this quantification are listed in Table S1 and Table S2.

The degree of crystallinity (DOC)[51], when the chemical composition of the crystalline phases are supposed identical to that of the whole sample, given as:

$$DOC = \frac{Crystalline\ area\ (wt\%)}{Amorphous\ area\ \ (wt\%)\ +\ Crystalline\ area\ (wt\%)} \qquad (4)$$

remains roughly 60% at 150°C and 275°C for K_2O/SiO_2=0.29 while an increase to 80% is observed at 350°C and 400°C. This behavior seems to be consistent with the plots in **Figure 2**(a) where the values of E_a tend to change above 330°C suggesting a direct link between the crystallization behavior and mass loss evolution. Details of the fitting parameters and the relative quantities of the crystalline and amorphous phases are given in Table S1. The

contribution from monoclinic $KHSi_2O_5$ decreases as a function of temperature while the orthorhombic phase increases until partial melting of the crystalline phases along with the appearance of crystalline K_2O is observed at 450°C. Quantification hasn't been done for the powder at 450°C due to a lack of availability of the crystallographic information file for various phases present at that particular temperature. Pre-dried K_2O/SiO_2=0.5, in contrast, is not crystallized during the 17 h long drying step (for solutions at 150°C) used for this study. However, longer drying duration (reaching 1 week) tends to favor crystallization with the formation of $KHSiO_3$ phase as shown in Figure S6(c).

Li-silicates are amorphous at 150°C and show both crystalline and amorphous character at and above 275°C as shown in **Figure 6**(b) for Li_2O/SiO_2=0.29 and Figure S7(b) for Li_2O/SiO_2=0.4. Two different crystalline phases, orthorhombic Li_2SiO_3 and $Li_2Si_2O_5$, are observed with a tendency towards increasing disilicate character suggesting the existence of the reaction: $Li_2SiO_3 + SiO_2 \rightarrow Li_2Si_2O_5$. The DOC increases from roughly 8% at 275°C to 50% at 450°C for Li_2O/SiO_2=0.29 while an increase in the crystalline character up to 400°C followed by a decrease due to partial melting of the crystalline phases is observed for Li_2O/SiO_2=0.29 (see Figure S7(b)). Here again, the fact that DOC remains in the range of 50% from 350°C to 450°C (depending upon the composition), crystallization seems to be directly linked to the existence of multiple and changing E_a values. Therefore, a direct consequence of crystallization seems to be a relatively suppressed macroscopic expansion both in K and Li-silicates (furthermore, phase separation in Li-silicates shouldn't be excluded).

These quantified values from the XRD data have allowed to calculate the relative fraction of alkali in the crystalline and amorphous phases at each temperature that may help in predicting the microstructural network evolution on thermal treatment. In order to provide

concrete information on the actual evolution of various proton and alkali-related species and their link to the foaming behavior, a combination of TGA, NMR and XRD data has thus been utilized to estimate the quantitative microstructural thermal evolution.

3.2.3. Variation of network modifiers

The starting aqueous alkali silicates are composed of large amounts of free water along with solvating water molecules and network silanols. As discussed earlier, the pre-drying step removes all the free water leaving behind a network containing silanols and H-bonded solvating water (note that the powders obtained by heat treatments at higher temperatures should gradually lose all proton-related species once the free water has been removed below 150°C). For a classification of these proton-related species, the following equation has to be considered:

$$\frac{Total\ Network\ Modifiers}{Si} = \frac{nM}{nSi} + \frac{nOH}{nSi} \tag{5}$$

where '*Total Network Modifiers*' refers to the species that contribute to the linkages with NBOs within the network, '*n*' represents the number of moles and '*M*' indicates the alkali ion. From TGA mass loss data, and assuming that all the proton-related species as well as alkali ions in the system are a part of the actual network, the '*Total Network Modifiers*' can be plotted as shown by the red curves in **Figure 7**. The concentration of alkali ion i.e. K or Li is already known and is shown by the blue lines. NMR data provides an exact quantification of the actual number of network modifiers shown in black and computed from the eq. 6 as:

$$\frac{Actual\ Network\ Modifiers}{Tetrahedra} = 4Q^0 + 3Q^1 + 2Q^2 + Q^3 \tag{6}$$

where Q^0 corresponds to a state where none of the oxygens of SiO_2 tetrahedra are connected to further Si atoms where as Q^1, Q^2 and Q^3 relates to the presence of 1, 2 and 3 bridged oxygens, respectively.

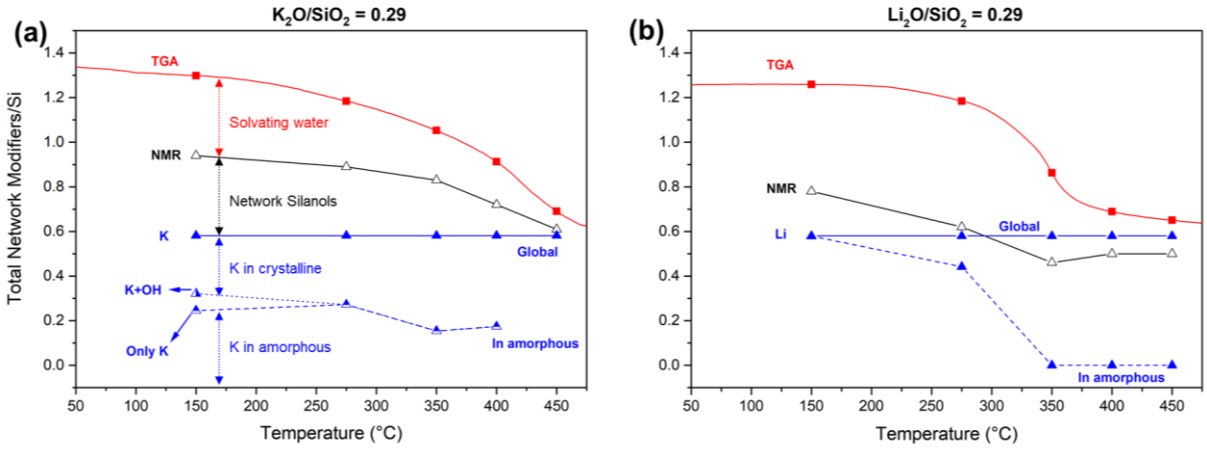

Figure 7: Evolution of Total Network Modifiers/Si as a function of temperature for (a) K_2O/SiO_2=0.29 and (b) Li_2O/SiO_2=0.29 extracted from a combination of TGA (solid red curve), ^{29}Si solid-state NMR (solid black curve) as well as powder XRD (dotted blue line) data.

The corresponding data for Na-silicates has been discussed in the previous work[11] where it was shown that solvating water and network silanols tend to evolve in parallel i.e. an equilibrium exists for their release with silanols condensing into solvating water followed by its evaporation, resulting in relatively extensive foaming as a consequence of the rapid and linear dehydration behavior (it should also be noted that Na-silicates do not crystallize below 500°C).

Since K_2O/SiO_2=0.29 tends to crystallize on thermal treatment (note that the kinetics of heating may influence the DOC) with the formation of $KHSi_2O_5$ crystallites suggesting that a part of total K ions leaves the amorphous phase, the quantity of alkali in the amorphous and crystalline phases is possible to be plotted from the quantified XRD data shown in **Figure 6**. For K_2O/SiO_2=0.29, the dashed blue line (with top filled triangles) in **Figure 7**(a) shows the

amount of K left in the amorphous phase after the formation of $KHSi_2O_5$ crystallites. The proportion of solvating water is marked with red, network silanols with black while K in crystalline or amorphous phase with blue arrows. It is worth noting that not all the network silanols at 150°C belong to the amorphous phase i.e. only a fraction of the total is linked to the amorphous network while the major chunk represents protons in the crystalline phase. On the contrary, K_2O/SiO_2=0.5 doesn't seem to crystallize as discussed before and, thus, a behavior similar to that for Na-silicates is observed as given in Figure S6(b). Note that the system would potentially crystallize on longer drying times, however, that has not been investigated extensively for this work (except for the point at 150°C).

Similar analysis for Li_2O/SiO_2=0.29 shown in **Figure 7**(b) (see Figure S7(c) for Li_2O/SiO_2=0.4) suggests a slightly different behavior than that observed for Na or K-silicate. The quantity of 'Actual Network Modifiers' from NMR data seems to cross the dashed blue line pointing to the fact that the network may not actually have all the Li as its component, rather some Li may well be in the form of LiOH as also evident from the liquid-state ^{29}Si NMR data in **Figure 4**(c) impacting directly the thermal evolution. Furthermore, crystallization of Li_2SiO_3 and $Li_2Si_2O_5$ should also remove some Li from the amorphous phase. The dashed blue line in **Figure 7**(b) gives the amount of Li remaining in the amorphous phase. Amorphous network of Li_2O/SiO_2=0.29 is Li free at 350°C similar to what is seen for Li_2O/SiO_2=0.4 (Figure S7(c)) where a minute quantity of Li ions is still intact within the amorphous phase. The increase in the quantity of Li seen for Li_2O/SiO_2=0.4 at 450°C in Figure S7(c) is a consequence of Q^2 (crystalline) + Q^4 (glassy) ↔ $2Q^3$ (glassy) reaction.

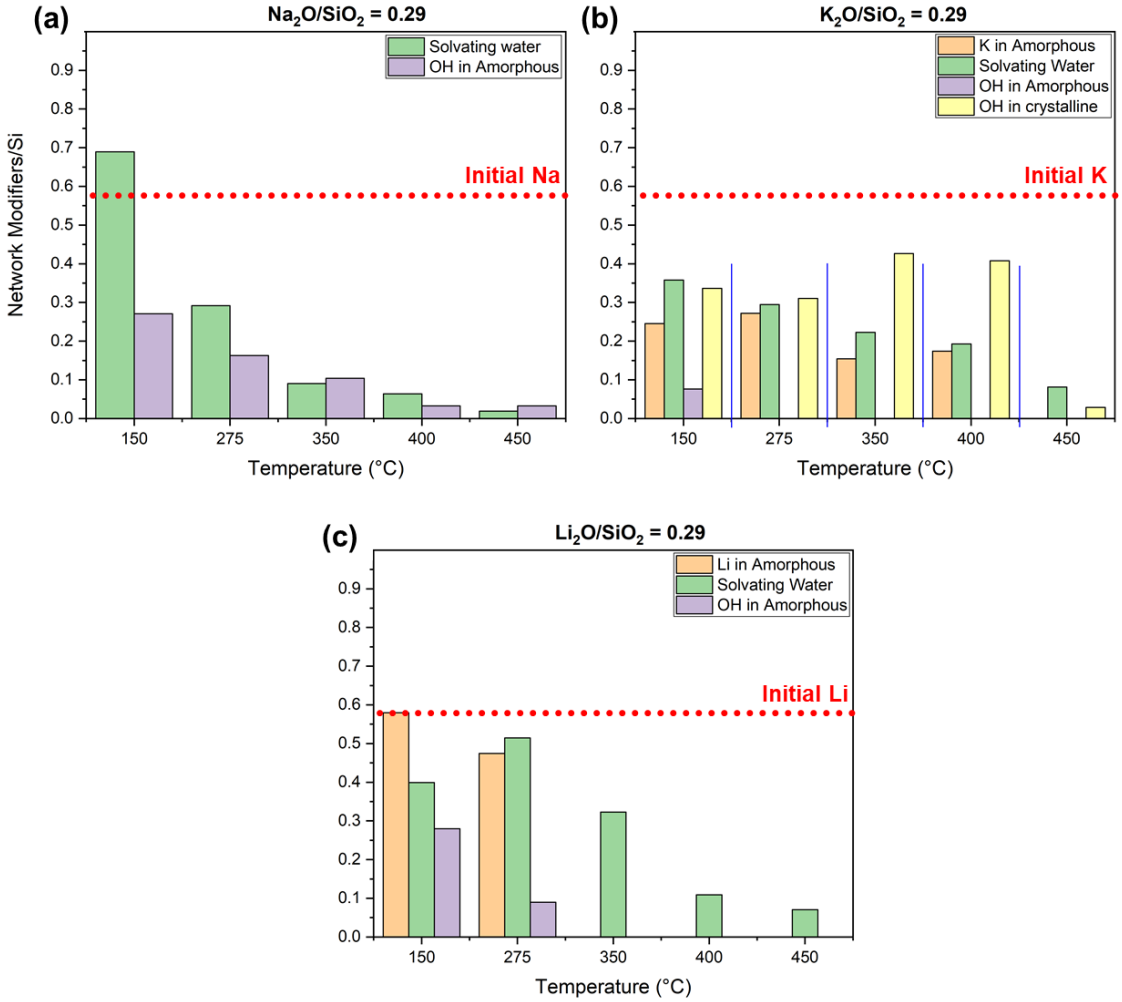

Figure 8: Quantitative thermal evolution of different species i.e solvating water, silanols (in amorphous or crystalline phase) and alkali ions for (a) Na (extracted from Figure 7 in ref [11]), (b) K and (c) Li-silicates extracted from the information given in Figures 5 and 6. The dotted line in red is indicative of the initial quantity of alkali ions. Note that Na-silicate doesn't exhibit any crystalline behavior and thus the alkali is expected to stay constant in the amorphous phase.

Figure 8 shows the quantitative evolution of the different species present in the system calculated from **Figure 7** for K and Li-silicate and Figure 7 in ref [11] for Na-silicate with molar ratio of 0.29. Evolution of solvating water is shown by green, silanols in the amorphous phase by purple, silanols in the crystalline phase by yellow and the amount of alkali remaining in the amorphous phase by orange bars. The red dotted line indicates the initial

quantity of alkali ions in the systems. For Na_2O/SiO_2=0.29, as evident from **Figure 8**(a), all the silanols are part of the amorphous network and evolve together with solvating water molecules as a function of temperature leading to extensive foaming. Similar behavior is observed for Na_2O/SiO_2=0.5 (data not shown here) with an increased quantity of solvating water molecules and silanols available in pre-dried powder at 150°C resulting in more volumetric expansion than Na_2O/SiO_2=0.29, mainly due to the higher network mobility imparted by the network modifiers either Na ions or protons.[11]

K and Li-silicates being crystallized show a different behavior for the evolution of the various species. It is worth recalling here that Na-silicates show an extensive macroscopic volumetric expansion in terms of foaming, Li-silicates don't foam at all while an intermediate behavior is observed for K-silicates (at a heating rate of 5°C/min). Since there is no crystallization or phase separation in Na-silicates rendering the network relatively mobile, the evolution of proton-related species results in maximum foaming.

The mobility of the network is reduced a lot in the case of Li-silicates. This stems from the fact that the starting compositions studied here lie in the phase separation regime (note that the starting solutions become whitish at rather lower temperatures i.e below 150°C as shown in Figure S5) when compared with the reported data for binary Li_2O-SiO_2 glass systems[23,27,32] indicating the formation of an almost pure SiO_2 phase. Although we do not have access to the phase separation diagram in the ternary system including water, it is likely that protons are mostly found in the Li-rich phase, since it is more thermodynamically favorable to cluster together network modifiers. A percolating (bi-continuous) SiO_2 phase results in a rigid system, preventing any expansion. On thermal treatment, apart from phase separation, the system tends to crystallize resulting in the loss of Li ions from the amorphous

phase. As can be seen from **Figure 7**(b) and **Figure 8**(c), all the Li ions leave the amorphous phase around 350°C rendering the amorphous network brittle. Furthermore, silanols in the amorphous network are also more or less removed between 275°C and 350°C, adding further to the rigidity of the network resulting in a mass that is not mobile enough to expand due to a very viscous nature, thus, suppressing the structure from expanding altogether. Solvating water is, therefore, mainly responsible for the mass loss observed in TGA shown in **Figure 2**. Moreover, the actual amount of solvating water molecules in Li-silicates, for instance, Li_2O/SiO_2=0.29 shown in **Figure 8**(c) could be a combination of solvating water as well as protons in LiOH. Since silanols are all lost at 350°C, solvating water molecules maybe linked to Q^2 and Q^3 crystalline phases as well as LiOH (especially above 275°C) or the LiOH molecules maybe H-bonded to the amorphous phase as indicated from the existence of amorphous Q^3 from ^{29}Si NMR data. Li_2O/SiO_2=0.4 shows a similar behavior in terms of the evolution of the different species and thus has a network mobility similar to Li_2O/SiO_2=0.29 resulting in no foaming.

K-silicate compositions are not in the phase separation regime; however, crystallization does appear on thermal treatment at temperatures as low as 150°C as shown in **Figure 6**(a), **Figure 7**(a) and **Figure 8**(b) for K_2O/SiO_2=0.29. It is worth noting here that direct heating of the K-silicate solutions (for instance at 10°C/min or higher) leads to extensive foaming especially for K_2O/SiO_2=0.29. However, heating at 1 to 5°C/min or drying of the systems at 150°C for a few hours may result in the formation of crystallites suppressing to a large extent the intumescent behavior of K-silicates (as evident from Figure S1 and in-situ hot-stage microscopy images in **Figure 1**(e)). Crystallization can reduce intumescence since the crystalline phase $KHSi_2O_5$ incorporates more potassium cations and protons than the average composition, reducing significantly the mobility, and also the water super-

saturation, of the amorphous phase. For pre-dried crystallized powders, crystalline content represents almost 60% of the total network configuration at 150°C and 275°C while the value goes up to 80% at 350°C and 400°C, however, all the K ions don't leave the amorphous phase at any point allowing for enough network mobility to be retained, although reduced, for the structure to expand slightly. The leftover silanols in the amorphous phase are all lost around 275°C while those in the crystalline phase remain more or less constant up to 400°C whereas solvating water molecules are lost gradually on increasing temperature representative of the mass loss in TGA curves (**Figure 2**). It is worth noting here that NMR data does not seem to give a precise measure of quantification for crystalline components. For instance, in **Figure 7**(a) the NMR NBOs/Si curve tends to reduce as a function of temperature and it might be suggestive of a decrease in the quantity of OH in the crystalline phase which happens to be not true according to the more accurate XRD data. This reduction might arise from the inability of NMR data to show exact quantification of the crystalline phases with respect to the amorphous part (due to the 8.4 T magnetic field strength used that may not be enough to have the best resolution). So, the yellow bars representing OH in the crystalline phase in **Figure 8**(b) correspond to the values computed from the deconvoluted XRD diffractograms given in **Figure 6**(a). Thus, the foaming/intumescent behavior for pre-dried K-silicate systems tends to be intermediate between Na and Li-silicates mainly due to the existence of enough network mobility at the beginning and throughout. Solvating water molecules appear to be linked to silanols in the amorphous phase (until 150°C), K ions in amorphous Q^3 and crystalline Q^3 phases. K_2O/SiO_2=0.5 (evolution not shown here) behaves in a manner similar to Na-silicates and a similar extensive foaming behavior may be expected. However, that is not the case as the system tends to be very hygroscopic i.e. water is thermodynamically more stable until 300°C

as shown by the phase diagram in **Figure 3**(d). Therefore, although the network is mobile as observed for Na-silicates, a behavior intermediate to Li and K-silicates is seen in terms of macroscopic evolution.

Literature report[10] on the thermal evolution of K-silicate solutions suggests the foaming of these systems to be a consequence of the evolution and amount of solvating water molecules. It could partly be true given the fact that silanols tend to convert into solvating water molecules due to the existence of an equilibrium between the two species as has been established for Na silicates. However, a more rigorous quantitative analysis using a combination of different tools (TGA, NMR and XRD) suggests that foaming happens to be a consequence of mainly network mobility and the amount of protons as silanols in the network, thus, allowing us to clearly distinguish among the various alkali types in terms of their foaming behavior. Moreover, the reported data available in literature concerns more the thick coatings developed from these aqueous solutions for which a study is ongoing to establish thermal evolution protocols as those established here for powders. Crystallization of a hydrated phase observed in pre-dried powders for K-silicates explains why water remains present at higher temperatures in the material, as evidenced by the TGA data (**Figure 2**(b)).

4. Conclusions

Intumescent behavior of alkali silicates is highly dependent upon the type of alkali ion and the starting composition. Heating silicate solutions to 350°C at a heating rate of 5°C/min shows extensive foaming in Na-silicates, no foaming in Li-silicates while an intermediate structural expansion in K-silicates. Thermally treating powders prepared by pre-drying solutions at 150°C shows that higher alkali content systems exhibit a lower initial

dehydration temperature. Multiple activation energies for both K and Li-silicates are observed mainly due to the formation of different crystalline phases confirmed by the deconvoluted solid-state ^{29}Si NMR as well as XRD data.

Na-silicate solutions do not crystallize on heating up to 500°C. K_2O/SiO_2=0.29 is crystallized even at 150°C with a DOC of 60% when dried for 17 h. Orthorhombic and monoclinic $KHSi_2O_5$ crystalline phases are formed that tend to evolve with temperature (DOC increases to around 80% at 400°C) until partial melting is observed at 450°C. Both Li-silicate molar ratios, on the other hand, are amorphous at 150°C while crystallization appears at 275°C with the formation of orthorhombic Li_2SiO_3 and $Li_2Si_2O_5$ phases. DOC increases as a function of temperature with the gradual conversion of Li_2SiO_3 into $Li_2Si_2O_5$. This crystallization behavior in K and Li-silicates has a direct impact on the macroscopic evolution of the silicates. Rietveld refinement of XRD diffractograms has helped in the deconvolution of the data that has aided in establishing a quantitative measure of the evolution of alkali ions and proton-related species.

Pre-dried Na-silicates have a gradual and continuous evolution of amorphous network silanols and solvating water molecules leading to extensive foaming stemming from the fact that the network is relatively mobile as well as water can leave the system easily. Amorphous silanols are lost altogether at 275°C for both K_2O/SiO_2=0.29 and Li-silicates while those linked to $KHSi_2O_5$ phase stay intact until 400°C. Intermediate intumescence in K-silicates is a result of the network mobility provided by K ions in the amorphous phase and the possibility of some solvating water molecules to be intact, however, crystallization reduces the foaming capacity. Li-silicates don't show any structural expansion as the studied compositions lie in the phase separation regime indicating the formation of a SiO_2 rich

matrix phase that opposes the structure from expanding. Crystallization at temperatures approaching 275°C leads to the removal of Li ions from the amorphous phase whereby all Li ions move into the crystalline counterpart at 350°C reducing further the already low mobility in Li-silicate systems, thus, preventing intumescence.

Our results also suggest that the degree of intumescence depends on the heating rate, through the degree of crystallization within the material.

5. Funding

This research did not receive any specific grant from funding agencies in the public, commercial, or not-for-profit sectors.

6. References

[1] E.M. Bulewicz, A. Pelc, R. Kozjowski, A. Miciukiewicz, Intumescent Silicate-based Materials: Mechanism of Swelling in Contact with Fire, Fire Mater. 9 (1985) 171–175.

[2] E.D. Weil, Fire-protective and flame-retardant coatings - A state-of-the-art review, J. Fire Sci. 29 (2011) 259–296. https://doi.org/10.1177/0734904110395469.

[3] E. Prud'Homme, P. Michaud, E. Joussein, J.M. Clacens, S. Arii-Clacens, I. Sobrados, C. Peyratout, A. Smith, J. Sanz, S. Rossignol, Structural characterization of geomaterial foams - Thermal behavior, J. Non. Cryst. Solids. 357 (2011) 3637–3647. https://doi.org/10.1016/j.jnoncrysol.2011.06.033.

[4] S. Delair, É. Prud'homme, C. Peyratout, A. Smith, P. Michaud, L. Eloy, E. Joussein, S. Rossignol, Durability of inorganic foam in solution: The role of alkali elements in the geopolymer network, Corros. Sci. 59 (2012) 213–221. https://doi.org/10.1016/j.corsci.2012.03.002.

[5] M. Strozi Cilla, P. Colombo, M. Raymundo Morelli, Geopolymer foams by gelcasting, Ceram. Int. 40 (2014) 5723–5730. https://doi.org/10.1016/j.ceramint.2013.11.011.

[6] G. Gettwert, W. Rieber, J. Bonarius, One-component silicate binder systems for coatings, Surf. Coatings Int. 81 (1998) 596–603.

[7] H.H. Weldes, R.K. Lange, Properties of soluble silicates, Ind. Eng. Chem. 61 (1969) 29–44. https://doi.org/https://doi.org/10.1021/ie50712a008.

[8] R.R. Petersen, J.F.S. Christensen, N.T. Jørgensen, S. Gustafson, L.A. Lindbjerg, Y. Yue, Preparation and thermal properties of commercial vermiculite bonded with potassium silicate, Thermochim. Acta. 699 (2021) 178926-. https://doi.org/10.1016/j.tca.2021.178926.

[9] K.B. Langille, D. Nguyen, J.O. Bernt, D.E. Veinot, M.K. Murthy, Mechanism of dehydration and intumescence of soluble silicates Part II Effect of the cation, J. Mater. Sci. 26 (1991) 704–710.

[10] K.B. Langille, D. Nguyen, J.O. Bernt, D.E. Veinot, M.K. Murthy, Mechanism of dehydration and intumescence of soluble silicates Part I Effect of silica to metal oxide molar ratio, J. Mater. Sci. 26 (1991) 695–703.

[11] H. Mohsin, S. Maron, I. Maurin, E. Burov, G. Tricot, L. Devys, E. Gouillart, T. Gacoin, Thermal behavior of waterglass: foaming and xerogel-to-glass evolution, J. Non. Cryst. Solids. 566 (2021) 120872-undefined. https://doi.org/10.1016/j.jnoncrysol.2021.120872.

[12] H. Roggendorf, D. Böschel, B. Rödicker, Differential scanning calorimetry at hydrothermal conditions of amorphous materials prepared by drying sodium silicate

solutions, J. Therm. Anal. Calorim. 63 (2001) 641–652. https://doi.org/10.1023/A:1010167415775.

[13] H. Roggendorf, D. Böschel, Hydrous sodium silicate glasses obtained by drying sodium silicate solutions, Glas. Sci. Technol. Glas. Berichte. 75 (2002) 103–111.

[14] N.-W. Lee, J.-W. Choi, J.-H. Kim, CHARACTERISTICS OF FIRE PROTECTIVE COATING THE TERNARY SOLUBLE SILICATE, in: Int. Symp. Fire Sci. Technol., 1997: pp. 120–129. https://www.koreascience.or.kr/article/CFKO199711921268748.page (accessed June 24, 2021).

[15] L. Xu, Y. Hu, Y. Mu, F. Zhang, J. Wang, W. Chen, Y. Li, C. Zu, Kinetics of foaming process of potassium silicate gel at high temperature, Mater. Lett. 281 (2020) 128614. https://doi.org/10.1016/j.matlet.2020.128614.

[16] L. Vidal, E. Joussein, M. Colas, J. Cornette, J. Sanz, I. Sobrados, J.L. Gelet, J. Absi, S. Rossignol, Controlling the reactivity of silicate solutions: A FTIR, Raman and NMR study, Colloids Surfaces A Physicochem. Eng. Asp. 503 (2016) 101–109. https://doi.org/10.1016/j.colsurfa.2016.05.039.

[17] W.J. Malfait, V.P. Zakaznova-Herzog, W.E. Halter, Quantitative Raman spectroscopy: High-temperature speciation of potassium silicate melts, J. Non. Cryst. Solids. 353 (2007) 4029–4042. https://doi.org/10.1016/j.jnoncrysol.2007.06.031.

[18] J.F. Stebbins, S. Sen, Oxide ion speciation in potassium silicate glasses: New limits from ^{17}O NMR, J. Non. Cryst. Solids. 368 (2013) 17–22. https://doi.org/10.1016/j.jnoncrysol.2013.02.024.

[19] H. Maekawa, T. Maekawa, K. Kawamura, T. Yokokawa, The structural groups of alkali

silicate glasses determined from ^{29}Si MAS-NMR, J. Non. Cryst. Solids. 127 (1991) 53–64.

[20] A. Masoudi Alavi, A. Sax, P. Quirmbach, Interaction of Aluminum Metaphosphates in the Setting of Potassium Silicate Solutions in Terms of the Crystalline Phase Composition., ChemistryOpen. 9 (2020) 631–636. https://doi.org/10.1002/open.202000060.

[21] H.R. Fernandes, D.U. Tulyaganov, M.J. Pascual, J.M.F. Ferreira, Structure-property relationships and densification-crystallization behaviours of simplified lithium disilicate glass compositions, Ceram. Int. 40 (2014) 129–140. https://doi.org/10.1016/j.ceramint.2013.05.113.

[22] P. Zhang, X. Li, J. Yang, S. Xu, The crystallization and microstructure evolution of lithium disilicate-based glass-ceramic, J. Non. Cryst. Solids. 392–393 (2014) 26–30. https://doi.org/10.1016/j.jnoncrysol.2014.03.020.

[23] P.. Soares, E.. Zanotto, V.. Fokin, H. Jain, TEM and XRD study of early crystallization of lithium disilicate glasses, J. Non. Cryst. Solids. 331 (2003) 217–227. https://doi.org/10.1016/j.jnoncrysol.2003.08.075.

[24] R.S. Soares, R.C.C. Monteiro, M.M.R.A. Lima, R.J.C. Silva, Crystallization of lithium disilicate-based multicomponent glasses - effect of silica/lithia ratio, Ceram. Int. 41 (2015) 317–324. https://doi.org/10.1016/j.ceramint.2014.08.074.

[25] S. Huang, B. Zhang, Z. Huang, W. Gao, P. Cao, Crystalline phase formation, microstructure and mechanical properties of a lithium disilicate glass-ceramic, J. Mater. Sci. 48 (2013) 251–257. https://doi.org/10.1007/s10853-012-6738-y.

[26] S. Huang, Z. Zujovic, Z. Huang, W. Gao, P. Cao, Crystallization of a high-strength lithium disilicate glass-ceramic: An XRD and solid-state NMR investigation, J. Non. Cryst. Solids. 457 (2017) 65–72. https://doi.org/10.1016/j.jnoncrysol.2016.11.015.

[27] G.A. Sycheva, Phase separation and crystallization in glasses of the lithium silicate system $xLi_2O \cdot (100 - X)SiO_2$ (x = 23.4, 26.0, 33.5), Glas. Phys. Chem. 37 (2011) 135–149. https://doi.org/10.1134/S1087659611020155.

[28] H. Pfeiffer, P. Bosch, S. Bulbulian, Synthesis of lithium silicates, J. Nucl. Mater. 257 (1998) 309–317.

[29] T. Tang, Z. Zhang, J.B. Meng, D.L. Luo, Synthesis and characterization of lithium silicate powders, Fusion Eng. Des. 84 (2009) 2124–2130. https://doi.org/10.1016/j.fusengdes.2009.02.017.

[30] P. Li, B.A. Ferguson, L.F. Francis, Sol-gel processing of lithium disilicate Part I Crystalline phase development of gel-derived powders, J. Mater. Sci. 30 (1995) 4076–4086.

[31] E.D. Zanotto, Effect of liquid phase separation on crystal nucleation in glass-formers. Case closed, Ceram. Int. 46 (2020) 24779–24791. https://doi.org/10.1016/j.ceramint.2020.06.305.

[32] J.E. Shelby, Property/Morphology Relations in Alkali Silicate Glasses, J. Am. Ceram. Soc. . 66 (1983) 754–757.

[33] D.E. Veinot, K.B. Langille, D.T. Nguyen, J.O. Bernt, Efflorescence of soluble silicate coatings, J. Non. Cryst. Solids. 127 (1991) 221–226.

[34] D. Massiot, F. Fayon, M. Capron, I. King, S. Le Calvé, B. Alonso, J.O. Durand, B. Bujoli, Z. Gan, G. Hoatson, Modelling one- and two-dimensional solid-state NMR spectra, Magn. Reson. Chem. 40 (2002) 70–76. https://doi.org/10.1002/mrc.984.

[35] A. Vaitkus, A. Merkys, S. Grazulis, Validation of the Crystallography Open Database using the Crystallographic Information Framework, J. Appl. Crystallogr. 54 (2021) 661–672. https://doi.org/10.1107/S1600576720016532.

[36] A. Jain, S.P. Ong, G. Hautier, W. Chen, W.D. Richards, S. Dacek, S. Cholia, D. Gunter, D. Skinner, G. Ceder, K.A. Persson, Commentary: The materials project: A materials genome approach to accelerating materials innovation, APL Mater. 1 (2013) 011002-1-011002–11. https://doi.org/10.1063/1.4812323.

[37] S. Zietka, J. Deubener, H. Behrens, R. Müller, Glass transition and viscosity of hydrated silica glasses, Phys. Chem. Glas. Eur. J. Glas. Sci. Technol. B,. 48 (2007) 380–387.

[38] J. Deubener, R. Müller, H. Behrens, G. Heide, Water and the glass transition temperature of silicate melts, J. Non. Cryst. Solids. 330 (2003) 268–273. https://doi.org/10.1016/S0022-3093(03)00472-1.

[39] A. Shen, H. Keppler, Infrared spectroscopy of hydrous silicate melts to 1000 °C and 10 kbar: direct observation of H_2O speciation in a diamond-anvil cell, Am. Mineral. 80 (1995) 1335–1338. https://doi.org/10.2138/am-1995-11-1223.

[40] M. Nowak, H. Behrens, The speciation of water in haplogranitic glasses and melts determined by in situ near-infrared spectroscopy, Geochim. Cosmochim. Acta. 59 (1995) 3445–3450.

[41] C.W. Bale, P. Chartrand, S.A. Degterov, G. Eriksson, K. Hack, R. Ben Mahfoud, J.

Melanqon, A.D. Pelton, S. Petersen, FactSage Thermochemical Software and Databases, Calphad. 26 (2002) 189–228. https://doi.org/https://doi.org/10.1016/S0364-5916(02)00035-4.

[42] I.L. Svensson, S. Sjöberg, L.-O. Öhman, Polysilicate equilibria in concentrated sodium silicate solutions, J. Chem. Soc., Faraday Trans. I. 82 (1986) 3635–3646.

[43] R.K. Harris, E.K.F. Bahlmann, K. Metcalfe, E.G. Smith, Quantitative silicon-29 NMR investigations of highly concentrated high-ratio sodium silicate solutions, Magn. Reson. Chem. 31 (1993) 743–747.

[44] A. V McCormick, A.T. Bell, C.J. Radke, Quantitative determination of siliceous species in sodium silicate solutions by ^{29}Si n.m.r. spectroscopy, Zeolites. 7 (1987) 183–190.

[45] S.D. Kinrade, D.L. Pole, Effect of alkali-metal cations on the chemistry of aqueous silicate solutions, Inorg. Chem. 31 (1992) 4558–4563. https://pubs.acs.org/sharingguidelines.

[46] J.L. Bass, G.L. Turner, Anion distributions in sodium silicate solutions. Characterization by ^{29}Si NMR and infrared spectroscopies, and vapor phase osmometry, J. Phys. Chem. B. 101 (1997) 10638–10644. https://pubs.acs.org/sharingguidelines.

[47] A. Gharzouni, E. Joussein, B. Samet, S. Baklouti, S. Pronier, I. Sobrados, J. Sanz, S. Rossignol, The effect of an activation solution with siliceous species on the chemical reactivity and mechanical properties of geopolymers, J. Sol-Gel Sci. Technol. 73 (2015) 250–259. https://doi.org/10.1007/s10971-014-3524-0.

[48] L. Vidal, A. Gharzouni, E. Joussein, M. Colas, J. Cornette, J. Absi, S. Rossignol, Determination of the polymerization degree of various alkaline solutions: Raman

investigation, J. Sol-Gel Sci. Technol. 83 (2017) 1–11. https://doi.org/10.1007/s10971-017-4394-z.

[49] A.S. Brykov, V. V. Danilov, E.Y. Aleshunina, State of silicon in silicate and silica-containing solutions and their binding properties, Russ. J. Appl. Chem. 81 (2008) 1717–1721. https://doi.org/10.1134/S1070427208100029.

[50] C. Bischoff, H. Eckert, E. Apel, V.M. Rheinberger, W. Höland, Phase evolution in lithium disilicate glass-ceramics based on non-stoichiometric compositions of a multi-component system: Structural studies by ^{29}Si single and double resonance solid state NMR, Phys. Chem. Chem. Phys. 13 (2011) 4540–4551. https://doi.org/10.1039/c0cp01440k.

[51] I.C. Madsen, N.V.Y. Scarlett, A. Kern, Description and survey of methodologies for the determination of amorphous content via X-ray powder diffraction, Zeitschrift Fur Krist. 226 (2011) 944–955. https://doi.org/10.1524/zkri.2011.1437.